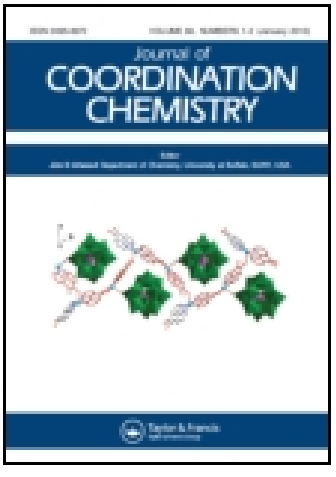

Journal of Coordination Chemistry
Publication details, including instructions for authors and subscription information:
http://www.tandfonline.com/loi/gcoo20

Synthesis of nickel(II) complexes of isatin thiosemicarbazone derivatives: in vitro anti-cancer, DNA binding, and cleavage activities

Amna Qasem Ali[a], Siang Guan Teoh[a], Naser Eltaher Eltayeb[b], Mohamed B. Khadeer Ahamed[c] & Ams Abdul Majid[c]

[a] School of Chemical Sciences, Universiti Sains Malaysia, Minden, Malaysia

[b] Department of Chemistry, Sciences & Arts College - Rabigh, King Abdulaziz University, Rabigh, Saudi Arabia

[c] EMAN Research and Testing Laboratory, School of Pharmaceutical Sciences, Universiti Sains Malaysia, Minden, Malaysia

Accepted author version posted online: 03 Sep 2014.Published online: 01 Oct 2014.

To cite this article: Amna Qasem Ali, Siang Guan Teoh, Naser Eltaher Eltayeb, Mohamed B. Khadeer Ahamed & Ams Abdul Majid (2014) Synthesis of nickel(II) complexes of isatin thiosemicarbazone derivatives: in vitro anti-cancer, DNA binding, and cleavage activities, Journal of Coordination Chemistry, 67:20, 3380-3400, DOI: 10.1080/00958972.2014.959943

To link to this article: http://dx.doi.org/10.1080/00958972.2014.959943

Journal of Coordination Chemistry, 2014
Vol. 67, No. 20, 3380–3400, http://dx.doi.org/10.1080/00958972.2014.959943

Synthesis of nickel(II) complexes of isatin thiosemicarbazone derivatives: *in vitro* anti-cancer, DNA binding, and cleavage activities

AMNA QASEM ALI†, SIANG GUAN TEOH*†, NASER ELTAHER ELTAYEB‡, MOHAMED B. KHADEER AHAMED§ and AMS ABDUL MAJID§

†School of Chemical Sciences, Universiti Sains Malaysia, Minden, Malaysia
‡Department of Chemistry, Sciences & Arts College – Rabigh, King Abdulaziz University, Rabigh, Saudi Arabia
§EMAN Research and Testing Laboratory, School of Pharmaceutical Sciences, Universiti Sains Malaysia, Minden, Malaysia

(*Received 18 March 2014; accepted 25 July 2014*)

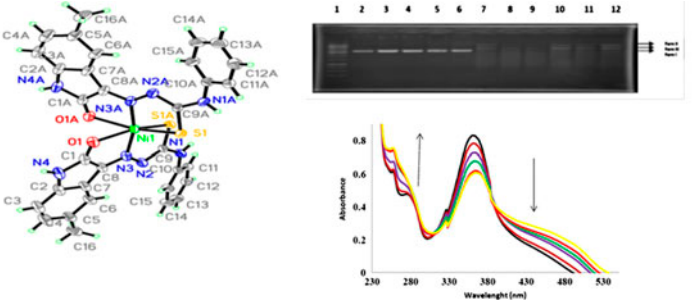

Six new nickel(II) complexes of thiosemicarbazone Schiff base with isatin moiety $[Ni(L1)_2–Ni(L6)_2]$ were synthesized through reaction of Ni(II) with (Z)-2-(2-oxoindolin-3-ylidene)-N-phenylhydrazinecarbothioamide (L1H), (Z)-2-(5-methyl-2-oxoindolin-3-ylidene)-N-phenylhydrazinecarbothioamide (L2H), (Z)-2-(5-fluoro-2-oxoindolin-3-ylidene)-N-phenylhydrazinecarbothioamide (L3H), (Z)-N-methyl-2-(5-nitro-2-oxoindolin-3-ylidene)hydrazinecarbothioamide (L4H), (Z)-N-methyl-2-(5-methyl-2-oxoindolin-3-ylidene)hydrazinecarbothioamide (L5H), and (Z)-N-ethyl-2-(5-methyl-2-oxoindolin-3-ylidene)hydrazinecarbothioamide (L6H). The structures of the Ni complexes were characterized through elemental analysis, infrared, and mass spectral data. The structure of the NiL2 complex was further characterized through single-crystal X-ray diffraction. The interaction of these complexes with calf thymus (CT-DNA) exhibited high intrinsic binding constants ($K_b = 1.4 \times 10^5$–2.4×10^6 M^{-1}), which reflected their intercalative activity toward CT-DNA. This result was also confirmed by viscosity data. Electrophoresis studies revealed that these complexes could cleave the DNA through the oxidative pathway. The *in vitro* anti-proliferative study establishes the anticancer potency of these compounds against human colorectal carcinoma cell line.

Keywords: Nickel(II) complexes; Isatin moiety; Intercalative activity; Oxidative pathway; Anti-proliferative activity

*Corresponding author. Email: sgteoh@usm.my

1. Introduction

Isatin thiosemicarbazones have numerous chemotherapeutic properties, such as anticancer, antimicrobial, antituberculosis, antiulcer, antiviral, antiplasmodial, cytotoxic, and enzymatic inhibition [1–12]. The biological activities of some thiosemicarbazone derivatives are related to their ability to form chelates with transition metal ions through O, N, and S. Metal ions are attracted to electron-rich molecules, such as proteins and DNA, leading to cleavage of DNA [13], mutagenesis, and cancer [14]. Transition metal elements have functions in medicinal chemistry, coordinating with different ligands to participate in biological redox chemistry. The metal in the complex also increases the overall activity compared to the free ligand. Nickel is an essential element for biological systems and is present in trace quantities for bacteria, plants, animals, and humans and has an essential function in certain enzymes such as urease. However, the biochemical activity of nickel has not been fully explored, and nickel complexes have been rarely studied in medicinal biochemistry [15]. Nickel(II) Schiff base complexes containing sulfur donors have received attention due to identification of a sulfur-rich coordination environment in biological nickel centres, such as the active sites of certain ureases, methyl-S-coenzyme-M-methyl reductase, and hydrogenases [16]. The known biological activity of nickel includes antiepileptics, anticonvulsant agents, vitamins, antibacterial, antifungal, antimicrobial, and anticancer/antiproliferative activities. Several reports have described the reactivity of DNA with mononuclear nickel(II) complexes [17]. The chemistry of nickel complexes with multidentate Schiff base ligands has attracted attention because such complexes play an important role in bioinorganic chemistry and redox enzyme systems, and may provide the basis for models of the active sites of biological systems or act as catalysts [18]. Our studies focused on the synthesis, physicochemical characterization, DNA binding, and nuclease activities of mononuclear Ni(II) complexes with tridentate ligands. The *in vitro* cytotoxic activities of the compounds were tested against human colorectal carcinoma cell line (HCT 116). The structures were proven through IR and mass spectroscopy. The single-crystal X-ray structure of the nickel complex $C_{32}H_{26}NiN_8O_2S_2$, $[Ni(L2)_2]$ was determined to confirm its structure. Several techniques were used to investigate the DNA-binding abilities of these complexes, including absorption, fluorescence spectrophotometry, and viscosity measurements. The nuclease activity with supercoiled (SC) pBR322 DNA was also examined. The *in vitro* cytotoxic activities of the compounds were tested against the human colorectal carcinoma cell line HCT 116.

2. Experimental

2.1. *Instruments*

The materials used in this study, such as isatin, 5-fluoroisatin, 5-methylisatin, 5-nitroisatin, 4-ethyl-3-thiosemicarbazide, 4-methyl-3-thiosemicarbazide, 4-phenyl-3-thiosemicarbazide, and nickel(II) chloride ($NiCl_2{\cdot}6H_2O$), were purchased from Aldrich Chemicals. Commercial-grade solvents and reagents were used as supplied without purification. SC pBR322 DNA and loading dye were purchased from Fermentas. Calf thymus [CT-DNA, agarose (molecular biology grade)] and ethidium bromide (EB) were from Sigma (St. Louis, MO, USA). 3-(4,5-Dimethylthiazol-2-yl)-2,5 diphenyl tetrazolium bromide (MTT) was purchased from Sigma-Aldrich, Germany. Elemental analysis was carried out using a Perkin-Elmer 2400 series-11 CHN/O analyzer (Waltham, MA, USA). The infrared, electronic, and

fluorescence spectra were recorded on Perkin-Elmer 2000, Perkin-Elmer Lambda 25, and Jasco FP-750 spectrophotometers, respectively. Viscosity measurements were carried out using a Cannon Manning semi-micro viscometer (State College, PA, USA). ESI-mass spectra were obtained through liquid chromatography/mass spectrometry using Trap VL (Agilent Technologies) operated in either positive ion or negative ion detection mode.

2.2. *Synthesis of ligands*

General procedure. The thiosemicarbazone derivatives (L1H–L6H) were previously synthesized and characterized in our laboratory [19–24]. Equimolar quantities of 5-unsubstituted or 5-substituted isatin were refluxed with thiosemicarbazide derivatives in ethanol for 2 h (scheme 1). The resulting precipitates were then filtered and washed with cold ethanol.

2.2.1. Synthesis of (*Z*)-2-(2-oxoindolin-3-ylidene)-*N*-phenylhydrazinecarbothioamide (L1H). $C_{15}H_{12}N_4OS$ (L1H): Yellow crystals; m.p.: 237.2–238.6 °C; yield: 90%; Anal. Calcd values: C (60.79%), H (4.08%), and N (18.91%); analytical results (experimental): C (60.50%), H (4.19%), and N (18.23%); selected IR data (KBr pellet, υ_{max}/cm^{-1}): 3300 to

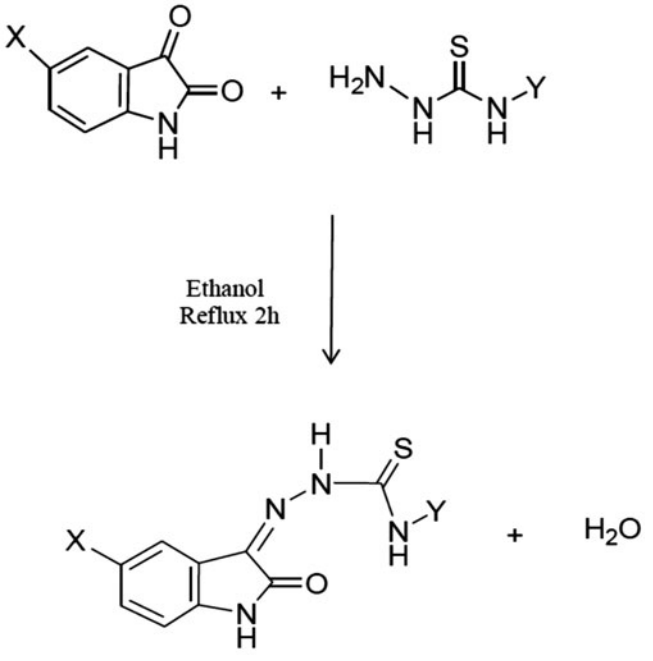

L1H) X = H, Y = Ph; L2H) X = CH_3, Y = Ph;
L3H) X = F, Y = Ph; L4H) X = NO_2, Y = CH_3;
L5H) X = Y = CH_3; L6H) X = CH_3, Y = CH_3CH_2

Scheme 1. Synthetic route and structures for the Schiff bases L1H–L6H.

3190 (NH), 1694 (C=O), 1621 (C=N), 1594 (C=C), 1138 (N–N), and 1208/790 (C=S); ^{1}H NMR (500 MHz, DMSO-d_6) [δ (ppm)]: 12.79 (s, 1 H, thiosemicarbazide N-NH),11.26 (s, 1 H, indole N–H), 10.98 (s, 1 H, CS-NH), 7.78 (d, 1 H, indole C2-H, J = 7.5 Hz), 7.62 (d, 2 H, thiosemicarbazide C11–H, C15–H, J = 7.7 Hz), 7.44–7.41 (t, 2 H, thiosemicarbazide C12-H, C14-H, J = 7.8), 7.39–7.36 (dt, 1 H, indole C3-H, J = 7.7, 1.0 Hz), 7.29–7.26 (t, 1 H, thiosemicarbazide C13-H, J = 7.4), 7.13–7.10 (t,1 H, indole C4-H, J = 7.5 Hz), 6.95 (d, 1 H, indole C5-H, J = 7.8); ^{13}C NMR (126 MHz, DMSO-d_6 ((δ (ppm)): 176.33, 162.68, 142.47, 138.43, 132.26, 131.41, 128.36, 126.07, 125.65, 124.65, 122.34, 121.37, 119.89, 111.07, and ESI-MS (*m/z*): 295(M^-).

2.2.2. Synthesis of (Z)-2-(5-methyl-2-oxoindolin-3-ylidene)-*N*-phenylhydrazine-carbothioamide (L2H). $C_{16}H_{14}N_4OS$ (L2H): Orange crystals; m.p.: 238.6–239.1 °C; yield: 80%; Anal. Calcd values: C (61.92%), H (4.55%), and N (18.05%); analytical results (experimental): C (61.89%), H (4.65%), and N (18.01%); selected IR data (KBr pellet, υ_{max}/cm^{-1}): 3308–3169 (NH), 1691 (C=O), 1627 (C=N), 1593 (C=C), 1135 (N–N), and 1212/762 (C=S); ^{1}H NMR (500 MHz, DMSO-d_6) [δ (ppm)]: 12.77 (s, 1 H, thiosemicarbazide N-NH), 11.15 (s, 1 H, indole N–H),10.81 (s, 1 H, CS–NH), 7.61 (d, 3 H, indole C5-H, thiosemicarbazide C11-H, C15-H, J = 7.7 Hz), 7.44–7.41 (t, 2 H, thiosemicarbazide C12-H, C14-H, J = 7.8 Hz), 7.29–7.26 (t, 1 H, thiosemicarbazide C13-H, J = 7.4 Hz), 7.19 (d,1 H, indole C3-H, J = 8 Hz), 6.84 (d, 1 H, indole C2-H, J = 7.9), 2.3 (s, 3 H, CH_3); ^{13}C NMR (126 MHz, DMSO-d_6 ((δ (ppm)): 176.30, 162.75, 140.25, 138.43, 132.37, 131.82, 131.36, 128.35, 126.06, 125.64, 121.74, 119.92, 110.82, 20.59, and ESI-MS *(m/z)*:309 (M^-).

2.2.3. Synthesis of (Z)-2-(5-fluoro-2-oxoindolin-3-ylidene)-*N*-phenylhydrazine-carbothioamide (L3H). $C_{15}H_{11}FN_4OS$ (L3H): Orange crystals; m.p.: 244.2–244.8 °C; yield: 77%; Anal. Calcd values: C (57.31%), H (3.52%), and N (17.82%); analytical results (experimental): C (57.42%), H (3.31%), and N (17.76%); selected IR data (KBr pellet, υ_{max}/cm^{-1}): 3313–3183 (NH), 1691 (C=O), 1594 (C=N), 1535 (C=C), 1140 (N–N), and 1202/797 (C=S); ^{1}H NMR (500 MHz, DMSO-d_6) [δ (ppm)]: 12.67 (s, 1 H, thiosemicarbazide N–NH), 11.26 (s, 1 H, indole N–H), 10.85 (s, 1 H, CS–NH), 7.65–7.63 (dd, 1 H, indole C3-H, J = 8.1, 2.6 Hz), 7.61 (d, 2 H, thiosemicarbazide C11-H, C15-H, J = 7.9 Hz), 7.45–7.42 (t, 2 H, thiosemicarbazide C12-H, C14-H, J = 7.8 Hz), 7.30–7.27 (t, 1 H, thiosemicarbazide C13-H, J = 7.4 Hz), 7.23–7.19 (dt, 1 H, indole C5-H, J = 7.7, 2.5 Hz), 6.95–6.93 (dd, 1 H, indole C2-H, J = 8.6, 4.1 Hz); ^{13}C NMR (126 MHz, DMSO-d_6 ((δ (ppm)): 176.79, 163.26, 159.69, 132.12, 128.92, 126.70, 126.12, 121.88, 121.81, 118.21, 118.01, 112.88, 112.61, 108.88, 108.68, and ESI-MS *(m/z)*: 313 (M^-).

2.2.4. Synthesis of (Z)-*N*-methyl-2-(5-nitro-2-oxoindolin-3-ylidene)hydrazinecarbothioamide (L4H). $C_{10}H_9N_5O_3S$ (L4H): Orange crystals; m.p.: 306.6–307.1 °C; yield: 80%; Anal. Calcd values: C (43.01%), H (3.25%), and N (25.08%); analytical results (experimental): C (43.12%), H (3.17%), and N (24.92%); Selected IR data (KBr pellet, υ_{max}/ cm^{-1}): 3437–3342 (NH), 1702 (C=O), 1623(C=N), 1551 (C=C), 1049 (N–N), and 1212/762 (C=S); ^{1}H NMR (500 MHz, DMSO-d_6) [δ (ppm)]: 12.32 (s, 1 H, thiosemicarbazide N–NH), 11.80 (s, 1 H, indole N–H), 9.53–9.50 (q, 1 H, CS–NH, J = 9.0, 4.5 Hz), 8.50 (d, 1 H, indole C5-H, J = 2.3 Hz), 8.25–8.23 (dd, 1 H, indole C3-H, J = 8.6, 2.5 Hz), 7.10

(d, 1 H, indole C2-H, $J = 8.6$ Hz), 3.40 (d, 3H, thiosemicarbazide CH_3, $J = 4.6$ Hz); ^{13}C NMR (126 MHz, DMSO-d_6 ((δ (ppm)): 177.54, 162.86, 147.19, 142.70, 129.47, 126.72, 120.92, 115.97, 111.15, 31.33, and ESI-MS *(m/z)*: 278 (M^-).

2.2.5. Synthesis of (Z)-*N*-methyl-2-(5-methyl-2-oxoindolin-3-ylidene)hydrazine-carbothioamide (L5H). $C_{11}H_{12}N_4OS$ (L5H): Yellow crystals; m.p.: 278.7–279.2 °C; yield: 94%; Anal. Calcd values: C (53.21%), H (4.87%), and N (22.56%); analytical results (experimental): C (53.45), H (4.21%), and N (22.51%); selected IR data (KBr pellet, υ_{max}/cm^{-1}): 3350–3248 (NH), 1693 (C=O), 1665(C=N), 1561 (C=C), 1042 (N–N), and 1205/791 (C=S); ^1H NMR (500 MHz, DMSO-d_6) [δ (ppm)]: 12.56 (s, 1 H, thiosemicarbazide N-NH), 11.09 (s, 1 H, indole N–H), 9.23–9.21 (q, 1 H, CS–NH, $J = 9.0$, 4.6 Hz), 7.50 (s, 1 H, indole C5-H), 7.16–7.14 (dd, 1 H, indole C3-H, $J = 7.9$, 0.9 Hz), 6.82 (d, 1 H, indole C2-H, $J = 7.9$ Hz), 3.09 (d, 3 H, thiosemicarbazide CH_3, $J = 4.6$ Hz), 2.30 (s, 3 H, indole CH_3); ^{13}C NMR (126 MHz, DMSO-d_6 ((δ (ppm)): 177.68, 162.65, 136.97, 131.64, 131.50, 131.31, 121.02, 119.98, 110.78, 31.27, 20.57, and ESI-MS *(m/z)*: 247 (M^-).

2.2.6. Synthesis of (Z)-*N*-ethyl-2-(5-methyl-2-oxoindolin-3-ylidenehydrazinecarbothioamide (L6H). $C_{12}H_{14}N_4OS$ (L6H): Yellow crystals; m.p.: 260.0–261.8 °C; yield: 80%; Anal. Calcd values: C (54.94%), H (5.38%), and N (21.36%); analytical results (experimental): C (54.83%), H (5.41%), and N (21.46%); selected IR data (KBr pellet, υ_{max}/cm^{-1}): 3343–3190 (NH), 1691 (C=O), 1669(C=N), 1543 (C=C), 1052 (N–N), and 1206/794 (C=S); ^1H NMR (500 MHz, DMSO-d_6) [δ (ppm)]: 12.53 (s, 1H, thiosemicarbazide N-NH), 11.09 (s, 1H, indole N–H), 9.28–9.25 (t, 1H, CS–NH, $J = 5.8$ Hz), 7.50 (s, 1 H, indole C5-H), 7.17 (d, 1 H, indole C2-H, $J = 7.9$ Hz), 6.83 (d, 1 H, indole C3-H, $J = 7.9$ Hz), 3.68–3.62 to (p, 2 H, thiosemicarbazide CH_2, $J = 6.8$ Hz), 2.31 (s, 3H, indole CH_3), 1.21–1.19 (t, 3H, thiosemicarbazide CH_3, $J = 7$); ^{13}C NMR (126 MHz, DMSO-d_6 ((δ (ppm)): 176.70, 162.66, 139.99, 131.70, 131.52, 131.29, 121.14, 119.98, 110.78, 40.11, 20.56, 14.00, and ESI-MS *(m/z)*: 263 (M^+).

2.3. *Synthesis of complexes*

The Ni(II) complexes were synthesized by refluxing the reaction mixture of hot ethanolic solutions (30 mL each) of $NiCl_2$ (0.01 M) and appropriate ligand (0.02 M) for 2 h. The precipitates that formed during the reflux were filtered and washed with cold ethanol (scheme 2).

2.3.1. Bis[2-(2-oxoindolin-3-ylidene)-*N*-phenylhydrazinecarbothioamidato-κ^3O,N^2,S]-nickel(II) dimethylformamide monosolvate [25]. $Ni(L1)_2$. $C_{30}H_{22}NiN_8O_2S_2$ [$Ni(L1)_2$]: Green crystal; m.p.: >300 °C; yield: 67%; Anal. Calcd values: C (55.49%), H (3.41%), N (17.26%), and Ni (9.04%); analytical results (experimental): C (55.67%), H (3.14%), N (16.93%), and Ni (9.20%); selected IR data (KBr pellet, υ_{max}/cm^{-1}): 3274–3134 (NH), 1668 (C=O), 1597 (C=N), 1048 (N–N), and 779 (C–S); UV–vis [DMSO, λ_{max}, nm, ε ($dm^3\ M^{-1}\ cm^{-1}$)]: 309.5 (10.0×10^3), 409.0 (10.0×10^3), and 505.0 (7.2×10^3); and ESI-MS (*m/z*): 649 $(M + H)^+$.

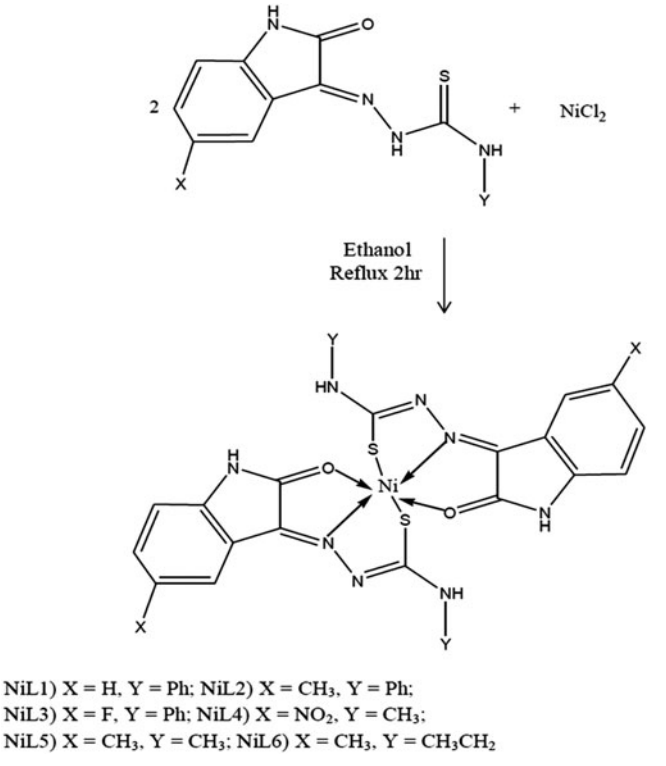

Scheme 2. Synthetic route and structures for NiL1–NiL6.

2.3.2. Bis[2-(5-methyl-2-oxoindolin-3-ylidene)-*N*-phenylhydrazinecarbothioamidato-κ^3*O*,*N*^{2},*S*]nickel(II). Ni(L2)$_2$. $C_{32}H_{26}NiN_8O_2S_2$ [Ni(L2)$_2$]: Reddish brown powder; m.p.: >300 °C; yield: 77%; Anal. Calcd values: C (56.74%), H (3.87%), N (16.54%), and Ni (8.66%); analytical results (experimental): C (56.96%), H (4.01%), N (16.64%), and Ni (8.90%); selected IR data (KBr pellet, υ_{max}/cm^{-1}): 3375–3276 (NH), 1669 (C=O), and 1595 (C=N), 1045 (N–N), and 750 (C–S); UV–vis [DMSO, λ_{max}, nm, ε (dm^3 M^{-1} cm^{-1})]: 306.0 (10.0 × 10^3), 408.5 (10.0 × 10^3), and 517.5 (10.0 × 10^3); and ESI-MS (*m/z*): 677 (M + H)$^+$.

2.3.3. Bis[2-(5-fluoro-2-oxoindolin-3-ylidene)phenylhydrazinecarbothioamidato-κ^3*O*, *N*^{2},*S*]-nickel(II). Ni(L3)$_2$. $C_{30}H_{20}NiF_2N_8O_2S_2$ [Ni(L3)$_2$]: Reddish brown powder; m.p.: >300 °C; yield: 80%; Anal. Calcd values: C (52.57%), H (2.94%), N (16.35%), and Ni (8.56%); analytical results (experimental): C (52.81%), H (3.12%), N (16.37%), and Ni (8.40%); selected IR data (KBr pellet, υ_{max}/cm^{-1}): 3407–3270 (NH), 1665 (C=O), 1595 (C=N), 1039 (N–N), and 749 (C–S); UV–vis [DMSO λ_{max}, nm, ε (dm^3 M^{-1} cm^{-1})]: 313.0 (10.0 × 10^3), 399.0 (10.0 × 10^3), and 477.5 (10.0 × 10^3); and ESI-MS (*m/z*): 685 (M + H)$^+$.

2.3.4. Bis[*N*-methyl-2-(5-nitro-2-oxoindolin-3-ylidene)hydrazinecarbothioamidato-κ^3*O*, *N*^{2},*S*]nickel(II). Ni(L4)$_2$. $C_{20}H_{16}NiN_{10}O_6S_2$ [Ni(L4)$_2$]: Reddish brown powder;

m.p.: >300 °C; yield: 83%; Anal. Calcd values: C (39.04%), H (2.62%), N (22.77%), and Ni (9.54%); analytical results (experimental): C (39.02%), H (2.48%), N (22.80%), and Ni (9.20%); selected IR data (KBr pellet, υ_{max}/cm^{-1}): 3341 (NH), 1661 (C=O), 1521 (C=N), 1029 (N–N), and 765 (C–S); UV–vis [DMSO λ_{max}, nm, ε ($dm^3\ M^{-1}\ cm^{-1}$)]: 311.0 (10.0×10^3), 402.5 (10.0×10^3), and 493.5 (5.7×10^3); and ESI-MS (*m/z*): 614 (M^-).

2.3.5. Bis[*N*-methyl-2-(5-methyl-2-oxoindolin-3-ylidene)hydrazinecarbothioamidato-κ^3*O*,*N*^{2},*S*]nickel(II). Ni(L5)$_2$. $C_{22}H_{22}NiN_8O_2S_2$ [Ni(L5)$_2$]: Reddish brown powder; m.p.: >300 °C; yield: 74%; Anal. Calcd values: C (47.76%), H (4.01%), N (20.25%), and Ni (10.61%); analytical results (experimental): C (47.43%), H (4.12%), N (20.42%), and Ni (10.42%); selected IR data (KBr pellet, υ_{max}/cm^{-1}): 3418–3295 (NH), 1651(C=O), 1513 (C=N), 1033 (N–N), and 745 (C–S); UV–vis [DMSO λ_{max}, nm, ε ($dm^3\ M^{-1}\ cm^{-1}$)]: 331.0 (10.0×10^3), 409.5 (10.0×10^3); and 471.5 (8.8×10^3); and ESI-MS (*m/z*): 552 $(M + H)^+$.

2.3.6. Bis[*N*-ethyl-2-(5-methyl-2-oxoindolin-3-ylidene)hydrazinecarbothioamidato-κ^3*O*, *N*^{2},*S*]nickel(II). Ni(L6)$_2$. $C_{24}H_{26}NiN_8O_2S_2$ [Ni(L6)$_2$]: Reddish-brown powder; m.p.: >300 °C; yield: 79%; Anal. Calcd values: C (49.58%), H (4.51%), N (19.28%), and Ni (10.10%); analytical results (experimental): C (49.86%), H (4.28%), N (19.14%), and Ni (10.36%); selected IR data (KBr pellet, υ_{max}/cm^{-1}): 3265 (NH), 1671 (C=O), 1599 (C=N), 1042 (N–N), and 749 (C–S); UV–vis [DMSO λ_{max}, nm, ε ($dm^3\ M^{-1}\ cm^{-1}$)]: 348.5 (10.0×10^3), 403.5 (10.0×10^3), and 434.5 (4.65×10^3); and ESI-MS (*m/z*): 581 $(M + H)^+$.

2.4. *X-ray crystallography*

Single crystals of Ni(L2)$_2$ suitable for diffraction were grown by slow evaporation of 3 : 1 mixtures of acetone and DMF. Ni(L2)$_2$ was crystallized with two molecules of DMF. Selected crystal data and data collection parameters are presented in table 1. The data of the Ni(L2)$_2$ complex were collected on a Bruker SMART APEX II CCD diffractometer [26] equipped with graphite monochromated Mo Kα radiation (λ = 0.71073) at 100(1) K. Multi-scan absorption corrections were applied using the SADABS program [26]. The structure was solved by direct methods using the SHELXS-97 program [27]. Refinements on F^2 were performed using SHELXL-97 by full-matrix least-squares with anisotropic thermal parameters for all non-hydrogen atoms. N-bound hydrogens were located in a difference Fourier map and were refined freely. The remaining hydrogens were positioned geometrically and refined using a riding model. SHELXTL [27] was used in the preparation of figure 1.

2.5. *DNA-binding studies*

DNA-binding experiments, which include absorption, emission spectral studies, and viscosity measurements, were performed in accordance with standard methods [28–30]. Concentrated CT-DNA stock solution was prepared in 5 mM Tris–HCl/50 mM NaCl in water at pH 7.2. The DNA concentration per nucleotide was determined by absorption spectroscopy using the molar absorption coefficient ($6600\ M^{-1}\ cm^{-1}$) at 260 nm [31]. The purity of the CT-DNA was verified by taking the ratio of the absorbance values at 260 and 280 nm in the respective buffer, always >1.9. This finding indicates that the DNA was sufficiently free of protein. The stock solutions were stored at 4 °C and used within 4 days. DNA-binding

Table 1. Crystallographic data for $Ni(L2)_2$.

Formula	$C_{32}H_{26}N_8NiO_2S_2$, C_4NO_2, C_3NO
Fw	837.53
Crystal system	Monoclinic
Space group	*C2/c*
a (Å)	22.161(3)
b (Å)	19.306(3)
c (Å)	10.6365(14)
α (°)	90
β (°)	115.222(2)
γ (°)	90
V (nm^3)	4116.9(10)
Z	4
D_{Calcd} (Mg m^{-3})	1.351
F (0 0 0)	1720
Crystal dimensions (mm)	0.102 × 0.269 × 0.681
θ range (°)	1.5, 30.0
hkl ranges	$-31 < h < 31$ $-27 < k < 27$ $-14 < l < 12$
Data/parameters	5980/270
Goodness-of-fit on F^2	1.04
Final *R* indices [$I > 2s(I)$]	$R_1 = 0.0678$ $wR_2 = 0.2104$
Highest peak/deepest hole	$\Delta\rho_{max} = 1.01e\,Å^{-3}/\Delta\rho_{min} = -0.96e\,Å^{-3}$

experiments were performed at room temperature. All experiments were carried out by keeping the concentration of nickel complexes constant (50 μM) while varying the DNA concentration (0–200 μM). An equal amount of DNA was added to the nickel complex cuvette and the reference cuvette to eliminate the absorbance of CT-DNA [32, 33]. Tris buffer was subtracted through baseline correction. The UV–vis and the emission spectra were recorded after equilibration for 10 min after each addition. Viscosity experiments were conducted using a Cannon Manning semi-micro viscometer (State College, PA, USA) and thermostated in a water bath maintained at 37.0 ± 0.1 °C. The flow rates of the Tris–HCl buffer (pH 7.2), CT-DNA (200 μM), and DNA in the presence of Ni(II) complex at various concentrations (0×10^{-4}–2.5×10^{-4} M) were measured three times each with a digital stopwatch, and the average flow time was calculated. The resulting data are presented as $(\eta/\eta_o)^{1/3}$ *versus*[complex]/[DNA], where η is the viscosity of the DNA in the presence of Ni (II) complex and η_o is the viscosity of the DNA. The viscosity values of DNA-containing solutions were calculated from the observed flow time (t) corrected from that of the buffer alone (Tris–HCl/NaCl, 5 : 50 mM) (t_o), $\eta = (t - t_o)$.

2.6. *DNA cleavage studies*

Cleavage experiments of SC pBR322 DNA (0.5 μg μL^{-1}) were performed at pH 7.2 in Tris–HCl/NaCl (5 : 50 mM) buffer. Oxidative DNA cleavage was monitored by treating pBR322 DNA with varying concentrations of Ni(II) complexes (0.1–1 mM) and H_2O_2, followed by dilution with Tris–HCl/NaCl (5 : 50 mM) buffer to a total volume of 20 μL (Lanes 4–12). To investigate the mechanism of DNA cleavage promoted by these complexes, the experiment was carried out by adding scavenger for reactive oxygen species (DMSO) to complex DNA mixture (Lane 3). The samples were incubated for 2 h at 37 °C. A loading dye was added, and electrophoresis was carried out at 50 V for 1 h in Tris–HCl

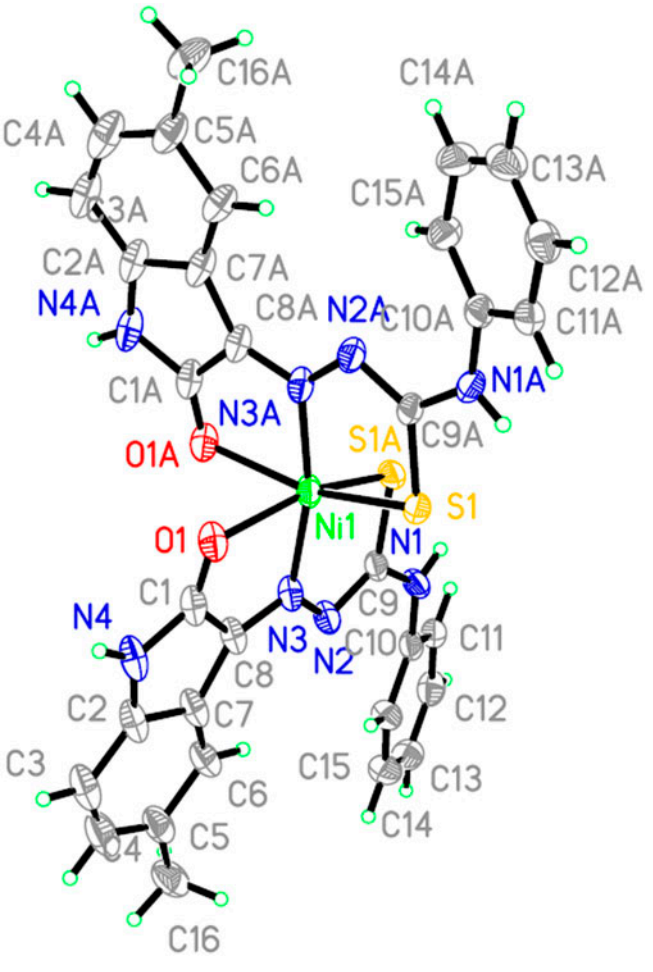

Figure 1. The structure of $Ni(L2)_2$ showing 50% probability displacement ellipsoids and atom numbering.

buffer using 1% agarose gel. The resulting bands were stained with EB before being photographed under UV light.

2.7. In vitro *anti-proliferative activity*

2.7.1. Preparation of cell culture. HCT 116 cells were allowed to grow under optimal incubator conditions. Cells that reached a confluence of 70–80% were chosen for cell plating. The old medium was aspirated out of the plate, and then, the cells were washed two to three times using sterile phosphate buffered saline (PBS; pH 7.4). PBS was discarded after washing. Trypsin was added and evenly distributed onto the cell surface, and the cells were incubated at 37 °C in 5% CO_2 for 1 min. Afterwards the flasks containing the cells were gently tapped to aid cell segregation and observed under an inverted microscope. If cell segregation was not satisfactory, the cells were incubated for another minute. Trypsin activity

was inhibited by adding 5 mL of fresh complete medium (10% FBS). Cells were counted and diluted to obtain a final concentration of 2.5×10^5 cells/mL and then seeded into wells (100 µL cells/well). Finally, the cell-containing plates were incubated at 37 °C with an internal atmosphere of 5% CO_2.

2.7.2. MTT assay. Cancer cells (100 µL cells/well, 1.5×10^5 cells/mL) were seeded on a 96-well microtiter plate incubated with CO_2 overnight to allow cell attachment. The compounds were diluted with media into the required concentrations from the stock. Various concentrations (6.25–200 µM) of 100 µL test substances were separately added to each well containing the cells. The plates were then incubated at 37 °C with an internal atmosphere of 5% CO_2 for 48 h. After the treatment period, the plates were treated with 20 µL of MTT reagent and incubated again for 4 h. After the incubation period, 50 µL of MTT lysis solution (DMSO) was added to the wells. The plates were further incubated for 5 min at room temperature. Finally, the absorbances at 570 and 620 nm were measured using a standard Infinite 200 PRO multimode microplate reader (Tecan, USA). Data were recorded and analyzed to estimate the effects of the test compounds on cell viability and growth inhibition. The percentage inhibition of cell proliferation was calculated from the optical density obtained from the MTT assay. 5-Fluorouracil (5-FU) was used as the standard reference drug [34]. Statistical difference between the treatments and the control was evaluated by one-way ANOVA, followed by Tukey's multiple comparison test. Differences were considered significant at $p < 0.05$ and $p < 0.01$.

3. Results and discussion

The nickel(II) complexes $Ni(L1)_2$–$Ni(L6)_2$ were obtained in good yield from the reaction of Ni(II) chloride with appropriate Schiff base (L1H–L6H) in 1 : 2 M ratio in ethanol with reflux for 2 h (via scheme 2). These complexes were slightly soluble in common organic solvents, but highly soluble in DMF and DMSO.

3.1. *Spectral characterization*

3.1.1. IR studies. Characteristic IR bands for the free ligands are different from those of the related complexes, providing significant indications regarding the bonding sites of the thiosemicarbazone ligands. Selected vibrational bands of the ligands and nickel complexes are listed in table 2. Compared with the spectra of the Schiff bases, all the Ni(II) complexes exhibit a band at 1651–1671 cm^{-1} assigned to ν(C=O). The shift of the band to lower wavenumbers indicates that the carbonyl oxygen is coordinated to the metal ion. The ν(C=N) band at 1513–1599 cm^{-1} in the metal complexes is shifted to lower wavenumbers, indicating that nitrogen of the azomethine group is coordinated. IR spectra of the free ligands have ν(N–N) at 1042–1149. This band shifted to lower wavenumbers (1029–1048) in spectra of the nickel complexes, indicating involvement of this group in complexation [35]. These compounds also display out-of-plane C–H bending and ring bending absorptions at 650–900 cm^{-1} [36]. The band corresponding to the C=S stretch appears at 762–797 cm^{-1} in the ligands spectra, lowered by ≈20 cm^{-1} in spectra of the complexes, indicating

Table 2. Selected vibrational bands of the ligand and its metal complexes.

Compound	*ν*C=O	*ν*C=N	*ν*N-N	*ν*C=S
L1H	1694	1621	1138	790
L2H	1691	1627	1135	762
L3H	1691	1625	1140	797
L4H	1702	1623	1049	785
L5H	1693	1629	1042	791
L6H	1691	1629	1052	794
$Ni(L1)_2$	1668	1597	1048	779
$Ni(L2)_2$	1669	1595	1045	750
$Ni(L3)_2$	1665	1595	1039	749
$Ni(L4)_2$	1661	1521	1029	765
$Ni(L5)_2$	1651	1513	1033	745
$Ni(L6)_2$	1671	1599	1042	749

involvement of the thioketo sulfur in coordination. The band that appears at 745–779 cm^{-1} is thus assigned to *ν*(C–S) in IR spectra of the metal complexes [37]. IR spectral results provide strong evidence for tridentate complexation of the Schiff base with nickel.

3.1.2. UV–vis studies. UV–vis absorption spectra of the Ni(II) complexes were measured from 200 to 800 nm using DMSO. Three absorptions with varying intensities can be observed. The bands observed from 306.0 to 348.5 nm are probably due to the intra-ligand $\pi \rightarrow \pi^*$ transitions of the thiosemicarbazone ligands. The bands from 399.0 to 409.5 nm can be attributed to ligand-to-metal charge transfer transitions from sulfur to nickel. Occurrence of $S \rightarrow M$ (LMCT) bands is quite common in electronic spectra of metal complexes of thiosemicarbazones. The bands at the lower frequency (434.5–517.5 nm) of the spectra correspond to d–d transitions [38, 39].

3.1.3. MS studies. The ESI-mass spectra of $Ni(L1)_2$, $Ni(L2)_2$, $Ni(L3)_2$, $Ni(L5)_2$, and $Ni(L6)_2$, which were recorded in positive mode, exhibit peaks at *m/z* 649, 677, 685, 552, and 581, respectively, indicating the presence of $[M + H]^+$ complexes. By contrast, the ESI-mass spectrum of $Ni(L4)_2$, which was recorded in negative mode, exhibit a peak at *m/z* 614, indicating the presence of $[M^-]$ complex. These assignments are based on ^{58}Ni. Further confirmation for the molecular structure of the investigated complexes comes from the appearance of other peaks containing ^{60}Ni besides the peaks due to successive degradation of the target compound to various fragments. Another confirmation came from the appearance of sodium adduct [M + Na + H] as in the case of $Ni(L4)_2$ (the peak at *m/z* 638). The data of the elemental analysis and MS for the prepared complexes confirm the stoichiometry of metal chelates as [ML2] type.

3.2. *Crystal structure description*

A crystal structure of $Ni(L1)_2$ has been published in our previous study [25]. The current study describes the crystal structure of $Ni(L2)_2$ and compares it with $Ni(L1)_2$. The asymmetric unit of the $Ni(L2)_2$ molecule (figure 1) contains one Ni(II) complex and two solvent molecules that may be DMF. The solvent molecules are disordered and not solved completely, but the crystal quality is good, with *R* value of 0.0678. This study will not discuss

these solvent molecules and concentrates on the Ni(II) complex. Coordination spheres around Ni(II) in both $Ni(L1)_2$ and $Ni(L2)_2$ are slightly distorted octahedral, with the coordination around Ni(II) formed by the S2N2O2 donors of the ligands. The Ni–O distance is 2.225 Å, with Ni–N distance of 2.003 Å and Ni–S distance of 2.370 Å, which fall in the range observed for $Ni(L1)_2$. For $Ni(L1)_2$, the Ni–O distances are 2.189–2.244 Å, with Ni–N distances of 2.034–2.037 Å and Ni–S distances of 2.356–2.387 Å.

The bond angle O1–Ni–O2 is 86.1°, S1–Ni–S2 is 94.9°, N1–Ni–N2 is 163°, S1–Ni–O1 is 160.7°, S2–Ni–O2 is 158.7°, and O1–Ni–N6 is 90°. These bond angles are comparable with that of $Ni(L2)_2$. Other bond lengths and angles observed in the structure are normal [40].

3.3. *DNA-binding studies*

3.3.1. Absorption spectral studies. One of the most useful techniques for DNA-binding studies of molecules is electronic absorption spectroscopy. DNA usually results in hypochromism and red shift (bathochromism) because of intercalation involving a strong stacking interaction between an aromatic chromophore and the DNA base pairs [41]. Hypochromism arises from the contraction of CT-DNA (calf thymus) in the helix axis and its conformational changes [42]. Meanwhile, hyperchromism results from the secondary damage of the DNA double helix structure [43, 44], in which the extent of hyperchromism is indicative of partial or non-intercalative binding modes [45]. The absorption spectra of 50 μM $Ni(L2)_2$ and $Ni(L3)_2$ complexes in the absence and presence of CT-DNA (0–200 μM) are given in figures 2 and 3. The absorption spectra of $Ni(L1)_2$, $Ni(L4)_2$, $Ni(L5)_2$, and $Ni(L6)_2$ are shown in Supplementary material (figures S1–S4, see online supplemental material at http://dx.doi.org/10.1080/00958972.2014.959943). Absorption spectra of $Ni(L1)_2$–$Ni(L6)_2$ display clear hypochromism with slight red shift of 2–7 nm. After intercalation of the compounds into the DNA base pairs, the π^* orbitals of the intercalated compounds are able to couple with the π orbitals of the base pairs, thereby decreasing the $\pi \rightarrow \pi^*$ transition energies [46]. These interactions result in the observed hypochromism [47]. The hypochromism of the complexes with aromatic thiosemicarbazone is in the order $Ni(L3)_2 > Ni(L2)_2 > Ni(L1)_2$, whereas the hypochromism of the compounds with aliphatic thiosemicarbazone is in the order $Ni(L5)_2 > Ni(L6)_2 > Ni(L4)_2$, which may be due to a strong stacking interaction between the aromatic chromophore of the ligand and the DNA base pairs [48]. Remarkably, the $Ni(L2)_2$ complex exhibits both hypochromism and hyperchromism at ~257 and 360 nm, respectively. This behavior has been reported for chiral Schiff base complexes [49, 50]. The entity of hyperchromism behavior [42, 43], which reflects the secondary damage in the complex ($Ni(L2)_2$), can be attributed to the enhanced hydrogen bonding between this complex and the DNA caused by the presence of an aliphatic group in the isatin moiety.

The intrinsic binding constants of all the complexes with DNA were obtained by observing the changes in the absorbance of the complexes with increase in DNA concentration using the following equation [51, 52]:

$$[\mathrm{DNA}]/(\varepsilon_a - \varepsilon_f) = [\mathrm{DNA}]/(\varepsilon_b - \varepsilon_f) + 1/K_b(\varepsilon_b - \varepsilon_f)$$

where ε_a, ε_f, and ε_b are the extinction coefficients observed for the absorption band at a given DNA concentration, free and bound complexes, respectively, and [DNA] is the concentration of DNA in the base pairs. The binding constant K_b was determined from the ratio

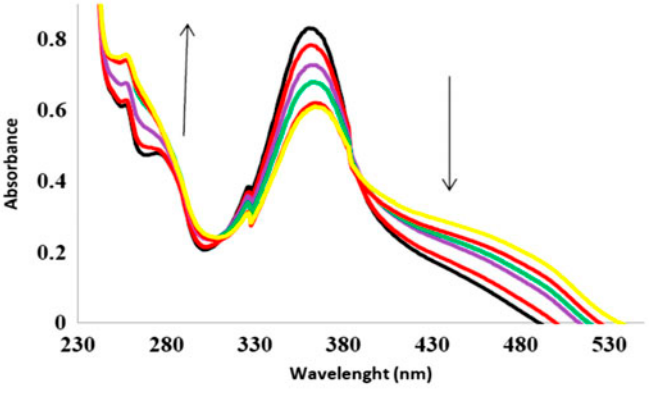

Figure 2. Absorption spectra of $Ni(L2)_2$ in the absence and presence of increasing amounts of DNA in Tris–HCl buffer (pH 7.2). $[Ni(L2)_2] = 50\,\mu M$, $[DNA] = 0–163.58 \times 10^{-6}$ M. The arrow shows the effect of increasing of CT-DNA concentration on the absorption intensity.

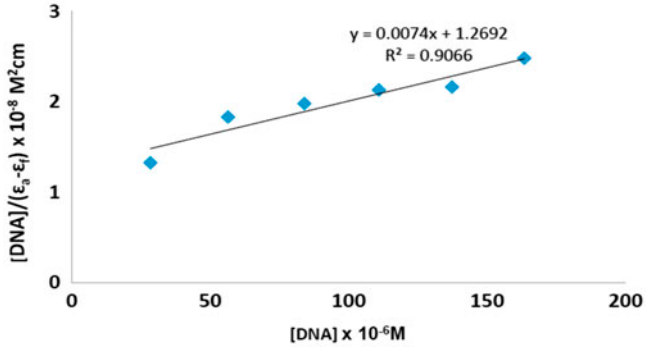

Figure 2a. Comparative plot of $[DNA]/(\varepsilon_a - \varepsilon_f)$ *vs.* [DNA] for the absorption titration of CT-DNA with $Ni(L2)_2$ in Tris–HCl buffer (pH 7.2); $K_p = 3.29 \times 10^6\ M^{-1}$ ($R = 0.9066$, $n = 6$ points).

of the slope to intercept by the $[DNA]/(\varepsilon_a - \varepsilon_f)$ *versus* [DNA] plot (figures 2a and 3a). The intrinsic binding constants (K_b) for $Ni(L1)_2$–$Ni(L6)_2$ were 7.39×10^5, 5.83×10^5, 1.07×10^6, 5.83×10^5, 1.41×10^5, and $2.44 \times 10^6\ M^{-1}$, respectively. Comparing the K_b values of these complexes with those of the DNA-intercalative Ni(II) complexes, such as the nickel complex of 6-hydroxy chromone-3-carbaldehyde thiosemicarbazone [53], $[Ni(sf)_2(bipyam)]\cdot 7H_2O$, $[Ni(oxo)_2(bipyam)]$, $[Ni(flmq)_2(bipyam)]$, and [Ni(erx)2(bipyam)] [54], these complexes can be assumed to bind to DNA by intercalation, but the binding mode needs to be proven through more experiments.

3.3.2. Emission spectral studies. To investigate further, the interaction mode among the Ni(II) complexes, $[Ni(L1)_2$–$Ni(L6)_2]$, and CT-DNA fluorescence titration experiments were performed. These complexes emit luminescence in Tris–HCl/NaCl buffer at room temperature with maximum wavelengths of approximately 379 nm (Supplementary material, figures S5–S8). The emission spectra of $Ni(L1)_2$ and $Ni(L2)_2$ (50 μM) in the absence and presence of CT-DNA (0–200 μM) are shown in figures 4 and 5. The emission intensity of

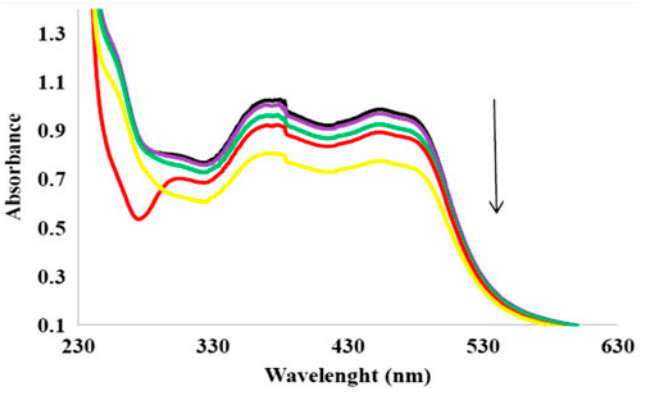

Figure 3. Absorption spectra of $Ni(L3)_2$ in the absence and presence of increasing amounts of DNA in Tris–HCl buffer (pH 7.2). $[Ni(L3)_2]$ = 50 µM, [DNA] = 0–163.58 × 10^{-6} M. The arrow shows the effect of increasing of CT-DNA concentration on the absorption intensity.

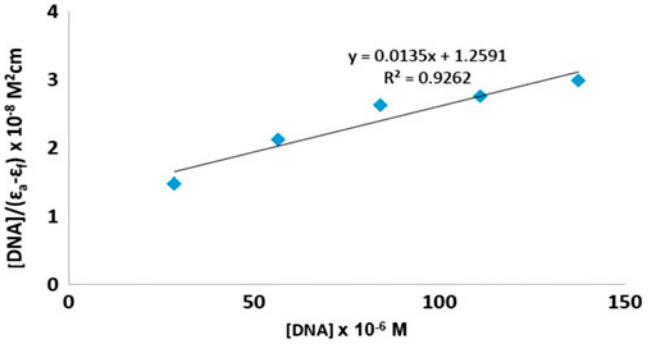

Figure 3a. Comparative plot of $[DNA]/(\varepsilon_a - \varepsilon_f)$ *vs.* [DNA] for the absorption titration of CT-DNA with $Ni(L3)_2$ in Tris–HCl buffer (pH 7.2); $K_p = 3.29 \times 10^6$ M^{-1} (R = 0.92621, n = 5 points).

$Ni(L1)_2$–$Ni(L6)_2$ increases with increasing CT-DNA concentrations. These observations imply that these complexes can strongly interact with CT-DNA and propose intercalative modes with the base pairs of the DNA helix [55].

3.3.3. Viscosity measurements. Hydrodynamic measurements (i.e. viscosity and sedimentation) that are sensitive to length changes are regarded as the most critical and the least ambiguous tests of binding in a solution in the absence of crystallographic data [56, 57]. A classical intercalator molecule such as EB can cause a significant increase in the viscosity of the DNA solution because of an increase in the separation of base pairs at the interaction site and an increase in overall double helix length. However, molecules that bind exclusively in the DNA grooves, groove face, or electrostatic interactions typically cause a bend in the DNA helix, thereby reducing its effective length and decreasing its viscosity [58–60]. The viscosity measurements of Ni complexes ($Ni(L1)_2$–$Ni(L6)_2$) and EB are shown in

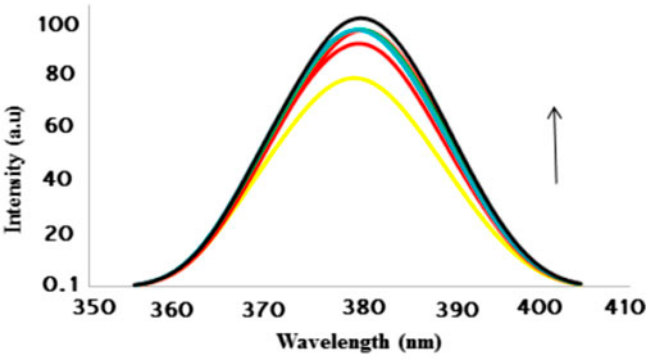

Figure 4. Emission spectra of $Ni(L1)_2$ in the absence and presence of increasing amounts of DNA in Tris–HCl buffer (pH 7.2). $[Ni(L1)_2]$ = 50 μM, [DNA] = 0–163.58 × 10^{-6} M. The arrow shows the emission intensity increases upon increasing CT-DNA concentration.

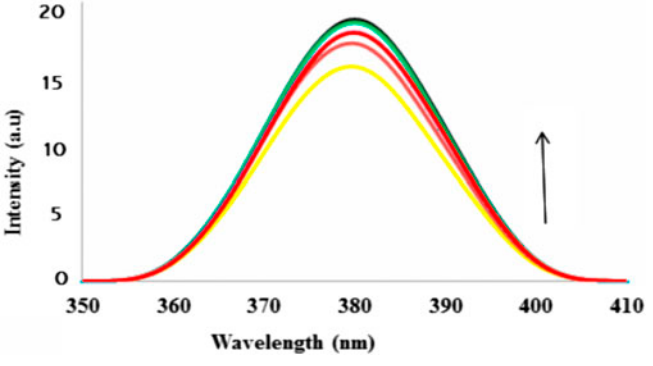

Figure 5. Emission spectra of $Ni(L2)_2$ in the absence and presence of increasing amounts of DNA in Tris–HCl buffer (pH 7.2). $[Ni(L2)_2]$ = 50 μM, [DNA] = 0–163.58 × 10^{-6} M. The arrow shows the emission intensity increases upon increasing CT-DNA concentration.

figures 6 and 7. The plot of relative specific viscosity *versus* [complex]/[DNA] ratio significantly increases upon the addition of ligand. These observations suggest the intercalative binding of these complexes to the double helix [61].

3.4. *DNA cleavage studies*

The cleavage of SC pBR322 DNA (0.5 μg μL^{-1}) was investigated through agarose gel electrophoresis using different concentrations of Ni(II) complexes (see Supplementary material, figures S9–S12) in 1% DMSO/5 mM Tris–HCl/50 mM NaCl buffer at pH 7.2, with and without H_2O_2, and with 2 h incubation. The activities of the complexes were estimated by the conversion of DNA from Form I to Forms II and III. The fastest migration is detected in the SC form (Form I). If only one strand is cleaved, the supercoils relax to convert into a slower-moving form (Form II). If both strands are cleaved, a linear form (Form III) is produced, which migrates between Forms I and II [62].

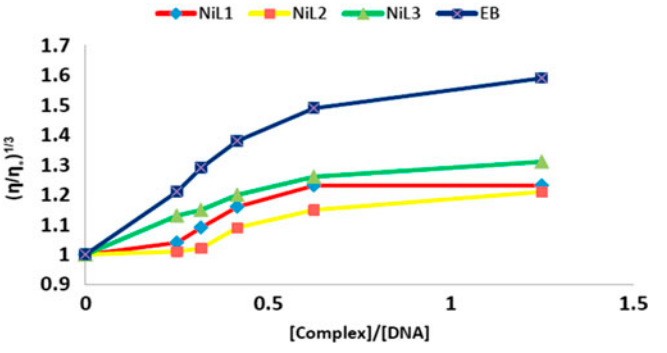

Figure 6. Effect of increasing amounts of EB (■), $Ni(L1)_2$ (■), $Ni(L2)_2$ (■), and $Ni(L3)_2$ (■) on the relative viscosity of CT-DNA at 37.0 (±0.1) °C.

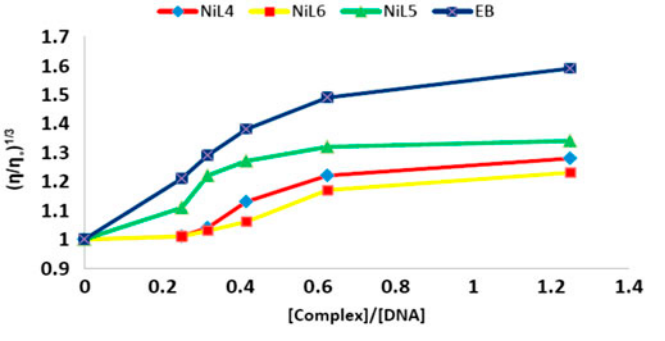

Figure 7. Effect of increasing amounts of EB (■), $Ni(L4)_2$ (■), $Ni(L5)_2$ (■), and $Ni(L6)_2$ (■) on the relative viscosity of CT-DNA at 37.0 (±0.1) °C.

3.5. *Oxidative cleavage*

The control experiment did not show any apparent cleavage of DNA (Lane 2). In the presence of the complexes [$Ni(L1)_2$–$Ni(L6)_2$] at different concentrations of H_2O_2 (Lanes 4–12), the plasmid DNA is converted from Form I to Form II at 0.1 mM concentration [Lane 4 for $Ni(L1)_2$, $Ni(L4)_2$, and $Ni(L5)_2$] and at 0.2 mM concentration [Lane 5 for ($Ni(L3)_2$), figure 8]. Meanwhile, the plasmid DNA is converted from Form I to Forms II and III at 0.1 and 0.4 mM concentrations [Lanes 4 and 7 for $Ni(L6)_2$ and $Ni(L2)_2$, respectively]. The DNA is totally degraded at 0.2, 0.3, 0.4, and 0.4 mM concentrations [Lanes 5, 6, 7, and 8 for Ni ($L6)_2$, $Ni(L4)_2$, $Ni(L5)_2$, and $Ni(L1)_2$, respectively]. These results indicate that the Ni(II) complexes can degrade pBR322 DNA through oxidative cleavage in the presence of H_2O_2 via the formation of hydroxyl radical species [63, 64]. This phenomenon can be explained by considering Fenton-type or Haber–Weiss-type reactions [65], in which a transition metal ion reduces H_2O_2 to yield hydroxyl radical that can damage the DNA and lead to strand breakage.

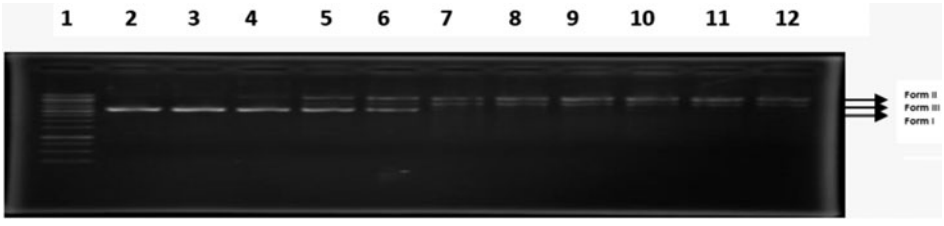

Figure 8. Cleavage of SC pBR322 (0.5 μg μL^{-1}) Ni(L3)$_2$ at different concentrations in Tris–HCl buffer pH (7.2) for 2 h at 37 °C. Lane 1: DNA ladder; Lane 2: DNA + H_2O_2; Lane 3: DNA + Ni(L3)$_2$ (1 mM) + DMSO; Lanes 4–12: DNA with increasing the concentrations of Ni(L3)$_2$ (0.1–1 mM) + H_2O_2 + 1% DMSO.

$$\mathrm{Ni(II)} + \cdot O_2^- \rightarrow \mathrm{Ni(I)} + O_2 \quad (1)$$

$$\mathrm{Ni(I)} + H_2O_2 \rightarrow \mathrm{Ni(II)} + OH^- + \cdot OH \quad (2)$$

$$\cdot O_2^- + H_2O_2 \rightarrow O_2 + OH^- + \cdot OH \quad (3)$$

To investigate the mechanism of DNA cleavage promoted by these complexes, the reactions were allowed to proceed in the presence of DMSO as hydroxyl radical scavengers (Lane 3). The addition of hydroxyl radical scavenger completely inhibits DNA cleavage activity (Ni(L5)$_2$, figure 9), which is induced by these complexes. This observation suggests the involvement of the hydroxyl radical in the cleavage [66], confirming the oxidative pathways of these complexes toward DNA [67]. The results revealed that the Ni(L6)$_2$ complex has more cleavage activity than the other complexes.

3.6. In vitro *anti-proliferative activity*

In vitro anti-proliferative study of the Ni(II) complexes of thiosemicarbazone analogs was previously conducted on Ehrlich ascitic carcinoma cells (IC_{50} = 191 μM) [66] against three human cancer cell lines (THP-1; IC_{50} = 89 μM, Raji; IC_{50} = 97 μM and Hela cells; IC_{50} = 181 μM) [52]. In the present research, the activities of the new Ni(II) complexes were studied against the human colorectal carcinoma cell line and are reported for the first time.

The *in vitro* anti-proliferative activity of the Ni(II) complexes of isatin thiosemicarbazone derivatives was evaluated against a human colorectal cancer (HCT116) cell. The effect of

Figure 9. Cleavage of SC pBR322 (0.5 μg μL^{-1}) Ni(L5)$_2$ at different concentrations in Tris–HCl buffer pH (7.2) for 2 h at 37 °C. Lane 1: DNA ladder; Lane 2: DNA + H_2O_2; Lane 3: DNA + Ni(L5)$_2$ (1 mM) + DMSO; Lanes 4–12: DNA with increasing the concentrations of Ni(L5)$_2$ (0.1–1 mM) + H_2O_2 + 1% DMSO.

different concentrations of Ni complexes [$Ni(L1)_2$–$Ni(L6)_2$] on human colorectal cancer cells (HCT 116) after 72 h of treatment is given in figure 10. The anticancer efficiencies of all tested compounds are presented in table 3. The cells treated with the standard drug 5-FU (IC_{50} = 7.3 μM) show strong inhibitory effect on cell proliferation. The cells exhibit several toxic signs, as all the cells are converted into round-shaped morphology after losing the normal pseudopodial cellular projections. These compounds show comparable cytotoxicities against HCT116 cell lines to those of 5-FU. Figure 11 shows the image of the cancer cells treated with these compounds for 48 h. The $Ni(L6)_2$ compound has the strongest cytotoxic effect (IC_{50} = 15 μM). The image shows clear signs of cytotoxicity of the compound on the cells, as most of the cells are affected because of the treatment. The effect can be compared with that of the standard reference 5-FU. The treatment of HCT 116 cells with the $Ni(L3)_2$ compound has significant cytotoxicity (IC_{50} = 55 μM). The population doubling time is reduced significantly compared with the negative control. The morphology of the cells reveals that the cells become weak because of the treatment. The HCT 116 cells treated with $Ni(L1)_2$ display moderate inhibition in cell proliferation, with IC_{50} = 79 μM. The image reveals that the number of cells considerably decreases compared with the negative control. The $Ni(L4)_2$ compound exhibits moderate inhibitory effect on the proliferation of

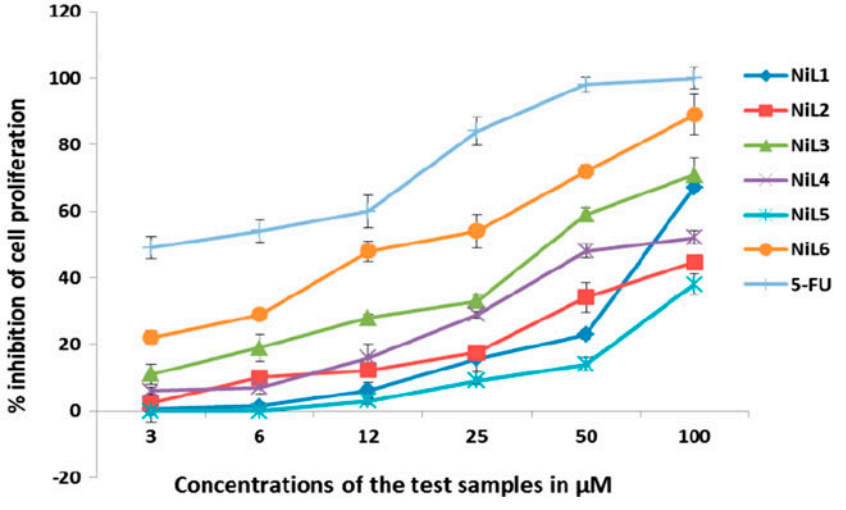

Figure 10. Effect of different concentrations of nickel(II) complexes of isatin thiosemicarbazone derivatives [$Ni(L1)_2$–$Ni(L6)_2$] on human colorectal cancer cells (HCT 116) after 72 h treatment.

Table 3. IC_{50} values of selected compounds.

Sample code	IC_{50} value/μM
$Ni(L1)_2$	79
$Ni(L2)_2$	104
$Ni(L3)_2$	55
$Ni(L4)_2$	85
$Ni(L5)_2$	134
$Ni(L6)_2$	15
5-FU	7.3

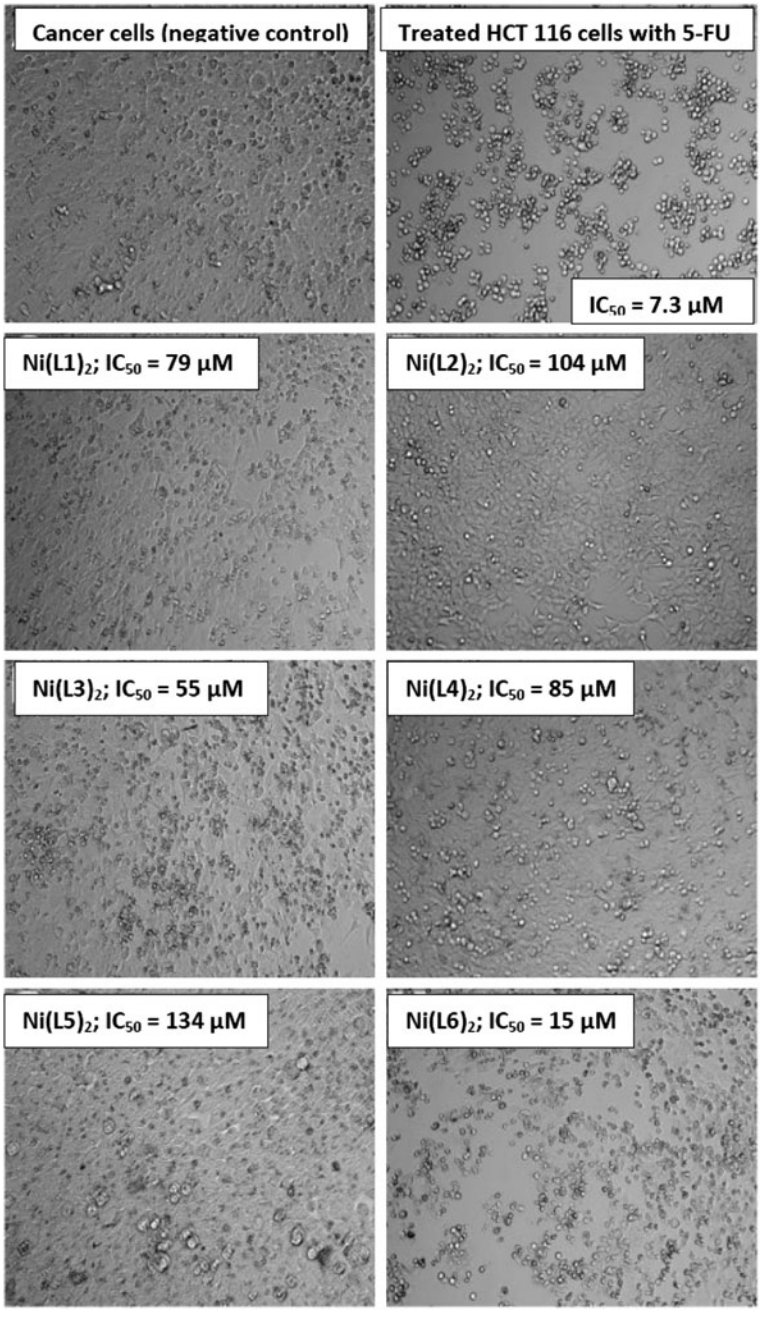

Figure 11. Picture of cancer cells treated with nickel(II) complexes of isatin thiosemicarbazone derivatives [Ni $(L1)_2$–Ni$(L6)_2$] for 48 h.

the cells (IC_{50} = 85 µM). Finally, compounds Ni$(L2)_2$ and Ni$(L5)_2$ show negligible cytotoxicity as the estimated IC_{50} is high (104 and 134 µM, respectively). The cellular morphology was unaltered compared with the vehicle-treated cells.

4. Conclusion

Six octahedral Ni(II) complexes, $Ni(L1)_2$–$Ni(L6)_2$, with tridentate ligands were synthesized and characterized using elemental analysis and various spectroscopic techniques. The crystal structure of $Ni(L2)_2$ showed that it was a six-coordinate complex with slightly distorted octahedral geometry. The results of binding studies showed that these complexes interact with CT-DNA through an intercalative mode, which was investigated by absorption (the intrinsic binding constant (K_b) values were 1.4×10^5–2.4×10^6 M^{-1}), fluorescence, and viscosity measurement. Finally, the results of the *in vitro* anti-proliferative activity against HCT 116 cells showed dose-dependent cytotoxicity of the synthesized complexes, with low IC_{50} values ranging from 15 to 134 μM. The strongest IC_{50} value for $Ni(L6)_2$ compared with $Ni(L1)_2$, $Ni(L2)_2$, and $Ni(L3)_2$, which have extended phenyl rings that may lead to additional activity, is unexpected [68]. The relationships between structure and anticancer potency are not yet well established. Elucidation of this behavior requires more experiments, which will be undertaken in the near future. The Ni(II) complexes of thiosemicarbazone Schiff bases with isatin can be promising anti-neoplastic agents. The toxic potentials of the most active complexes and their anti-tumor efficacies are under investigation in animal models, and will be reported in due course. The structure–activity relationship studies were recommended for future work.

Acknowledgements

The authors thank the Malaysian Government and Universiti Sains Malaysia for the RU research grant (1001/PKIMIA/815067).

References

[1] I. Chiyanzu, E. Hansell, J. Gut, P.J. Rosenthal, J.H. McKerrow, K. Chibale. *Bioorg. Med. Chem. Lett.*, **13**, 3527 (2003).
[2] G. Krishnegowda, A.S. Prakasha Gowda, H.R.S. Tagaram, K.F. Staveley-O'Carroll, R.B. Irby, A.K. Sharma, S. Amin. *Bioorg. Med. Chem.*, **19**, 6006 (2011).
[3] Pde M. Candido-Bacani, M.B. dos Reis, J.M. Serpeloni, T.R. Calvo, W. Vilegas, E.A. Varanda, I.M. Cólus. *Mutat. Res.*, **719**, 47 (2011).
[4] N. Karalı, Ö. Güzel, N. Özsoy, S. Özbey, A. Salman. *Eur. J. Med. Chem.*, **45**, 1068 (2010).
[5] L.-S. Feng, M.-L. Liu, B. Wang, Y. Chai, X.-Q. Hao, S. Meng, H.-Y. Guo. *Eur. J. Med. Chem.*, **45**, 3407 (2010).
[6] K. Karthikeyan, P.M. Sivakumar, M. Doble, P.T. Perumal. *Eur. J. Med. Chem.*, **45**, 3446 (2010).
[7] T.N. Akhaja, J.P. Raval. *Eur. J. Med. Chem.*, **46**, 5573 (2011).
[8] N. Siddiqui, M.S. Alam, J.P. Stables. *Eur. J. Med. Chem.*, **46**, 2236 (2011).
[9] G. Bhaskar, Y. Arun, C. Balachandran, C. Saikumar, P.T. Perumal. *Eur. J. Med. Chem.*, **51**, 79 (2012).
[10] V. Raj, V. Kumar, S. Kumar. *Int. J. Pharm. Integr. L. Sci.*, **4**, 30 (2013).
[11] H. Pervez, N. Saira, M.S. Iqbal, M. Yaqub, K.M. Khan. *Med. Chem. Res.*, **22**, 5878 (2013).
[12] G. Ermut, N. Karalı, İ. Çetin, M. Topçul, S. Birteksöz. *Marmara Pharm. J.*, **17**, 147 (2013).
[13] O.A. El-Gammal, I.M. Abd Al-Gader, A.A. El-Asmy. *Spectrochim. Acta, Part A*, **128**, 759 (2014).
[14] K. Tripathi. *Asian J. Res. Chem.*, **2**, 14 (2009).
[15] A. Ray, B.K. Seth, U. Pal, S. Basu. *Spectrochim. Acta, Part A*, **92**, 164 (2012).
[16] O.B. Ibrahim, M.A. Mohamed, M.S. Refat. *Can. Chem. Trans.*, **2**, 108 (2014).
[17] N. Selvakumaran, N.S.P. Bhuvanesh, A. Endo, R. Karvembu. *Polyhedron*, **75**, 95 (2014).
[18] B. Shafaatian, A. Soleymanpour, N.K. Oskouei, B. Notash, S.A. Rezvani. *Spectrochim. Acta, Part A*, **128**, 363 (2014).
[19] A.Q. Ali, N.E. Eltayeb, S.G. Teoh, A. Salhin, H.-K. Fun. *Acta Cryst.*, **E68**, o962 (2012).
[20] A.Q. Ali, N.E. Eltayeb, S.G. Teoh, A. Salhin, H.-K. Fun. *Acta Cryst.*, **E67**, o3476 (2011).

[21] A.Q. Ali, N.E. Eltayeb, S.G. Teoh, A. Salhin, H.-K. Fun. *Acta Cryst.*, **E68**, o285 (2012).
[22] A.Q. Ali, N.E. Eltayeb, S.G. Teoh, A. Salhin, H.-K. Fun. *Acta Cryst.*, **E68**, o953 (2012).
[23] A.Q. Ali, N.E. Eltayeb, S.G. Teoh, A. Salhin, H.-K. Fun. *Acta Cryst.*, **E68**, o955 (2012).
[24] A.Q. Ali, S.G. Teoh, A. Salhin, N.E. Eltayeb, M.K. Ahamed, A.M.S. Abdul Majid. *Spectrochim. Acta, Part A*, **125**, 440 (2014).
[25] A.Q. Ali, N.E. Eltayeb, S.G. Teoh, A. Salhin, H.-K. Fun. *Acta Cryst.*, **E68**, m538 (2012).
[26] Bruker. *APEX2, SAINT and SADABS*, Bruker AXS Inc., Madison, WI (2005).
[27] G.M. Sheldrick. *Acta Cryst.*, **A64**, 112 (2008).
[28] N. Mahalakshmi, R. Rajavel. *Asian J. Biochem. Pharm. Res.*, **2**, 525 (2011).
[29] W.C. Chen, L.D. Wang, Y.T. Li, Z.Y. Wu, C.W. Yan. *Transition Met. Chem.*, **37**, 569 (2012).
[30] A. Hussain, S. Gadadhar, T.K. Goswami, A.A. Karande, A.R. Chakravarty. *Eur. J. Med. Chem.*, **50**, 319 (2012).
[31] M.N. Dehkordi, A.K. Bordbar, P. Lincoln, V. Mirkhani. *Spectrochim. Acta, Part A*, **90**, 50 (2012).
[32] H. Paul, T. Mukherjee, M.G.B. Drew, P. Chattopadhyay. *J. Coord. Chem.*, **65**, 1289 (2012).
[33] Y. Li, Z.Y. Yang, M.F. Wang. *J. Fluoresc.*, **20**, 891 (2010).
[34] T. Mosmann. *J. Immunological Methods*, **65**, 55 (1983).
[35] M.B. Ummathur, D.K. Babu, K. Krishnankutty. *J. Serb. Chem. Soc.*, **79**, 303 (2014).
[36] R. Takjoo, M. Ahmadi, A. Akbari, H.A. Rudbari, F. Nicolò. *J. Coord. Chem.*, **65**, 3403 (2012).
[37] L.M. Chen, J. Liu, J.C. Chen, C.P. Tan, S. Shi, K.C. Zheng, L.N. Ji. *J. Inorg. Biochem.*, **102**, 330 (2008).
[38] V.M. Leovac, L.S. Jovanović, V. Divjaković, A. Pevec, I. Leban, T. Armbruster. *Polyhedron*, **26**, 49 (2007).
[39] S. Zhang, J. Dong, X. Fan, Y. Chen, J. Zhou. *J. Coord. Chem.*, **65**, 3098 (2012).
[40] F.H. Allen, O. Kennard, D.G. Watson, L. Brammer, A.G. Orpen, R. Taylor. *J. Chem. Soc., Perkin Trans. 2*, S1 (1987).
[41] C.Y. Zhou, J. Zhao, Y.B. Wu, C.X. Yin, P. Yang. *J. Inorg. Biochem.*, **101**, 10 (2007).
[42] S. Rajalakshmi, T. Weyhermüller, A.J. Freddy, H.R. Vasanthi, B.U. Nair. *Eur. J. Med. Chem.*, **46**, 608 (2011).
[43] R. Eshkourfu, B. Čobeljić, M. Vujčić, I. Turel, A. Pevec, K. Sepčić, M. Zec, S. Radulović, T. Srdić-Radić, D. Mitić, K. Andjelković, D. Sladić. *J. Inorg. Biochem.*, **105**, 1196 (2011).
[44] Ng. Lingthoingambi, N. Rajen Singh, M. Damayanti. *J. Chem. Pharm. Res.*, **3**, 187 (2011).
[45] L. Leelavathy, S. Anbu, M. Kandaswamy, N. Karthikeyan, N. Mohan. *Polyhedron*, **28**, 903 (2009).
[46] D.S. Raja, N.S.P. Bhuvanesh, K. Natarajan. *Inorg. Chim. Acta*, **385**, 81 (2012).
[47] N.H. Khan, N. Pandya, N.Ch Maity, M. Kumar, R.M. Patel, R.I. Kureshy, S.H.R. Abdi, S. Mishra, S. Das, H.C. Bajaj. *Eur. J. Med. Chem.*, **46**, 5074 (2011).
[48] N.H. Khan, N. Pandya, M. Kumar, P.K. Bera, R.I. Kureshy, S.H.R. Abdi, H.C. Bajaj. *Org. Biomol. Chem.*, **8**, 4297 (2010).
[49] S. Rajalakshmi, T. Weyhermüller, A.J. Freddy, H.R. Vasanthi, B.U. Nair. *Eur. J. Med. Chem.*, **46**, 608 (2011).
[50] K.C. Skyrianou, F. Perdih, A.N. Papadopoulos, I. Turel, D.P. Kessissoglou, G. Psomas. *J. Inorg. Biochem.*, **105**, 1273 (2011).
[51] N. Shahabadi, S. Kashanian, F. Darabi. *Eur. J. Med. Chem.*, **45**, 4239 (2010).
[52] B. Wang, Z. Yang, M. Lü, J. Hai, Q. Wang, Z. Chen. *J. Organomet. Chem.*, **694**, 4069 (2009).
[53] K.C. Skyrianou, F. Perdih, A.N. Papadopoulos, I. Turel, D.P. Kessissoglou, G. Psomas. *J. Inorg. Biochem.*, **105**, 1273 (2011).
[54] R. Palchaudhuri, P.J. Hergenrother. *Curr. Opin. Biotechnol.*, **18**, 497 (2007).
[55] M. Tarui, M. Doi, T. Ishida, M. Inoue, S. Nakaike, K. Kitamura. *Biochem. J.*, **304**, 271 (1994).
[56] H. Guo, J. Lu, Z. Ruan, Y. Zhang, Y. Liu, L. Zang, J. Jiang, J. Huang. *J. Coord. Chem.*, **65**, 191 (2012).
[57] L.B. Liaoa, H.Y. Zhou, X.M. Xiao. *J. Mol. Struct.*, **749**, 108 (2005).
[58] N. Raman, S. Sobha. *J. Serb. Chem. Soc.*, **75**, 773 (2010).
[59] S. Kashanian, M. Mehdi, K.P. Pakravan, H. Adibi. *Mol. Biol. Rep.*, **39**, 3853 (2012).
[60] F. Liu, K. Wang, G. Bai, Y. Zhang, L. Gao. *J. Inorg. Chem.*, **43**, 1799 (2004).
[61] P.P. Netalkar, A. Kamath, S.P. Netalkar, V.K. Revankar. *Spectrochim. Acta, Part A*, **97**, 762 (2012).
[62] L. Jin, P. Yang. *Microchem. J.*, **58**, 144 (1998).
[63] N. Raman, K. Pothiraj, T. Baskaran. *J. Coord. Chem.*, **64**, 3900 (2011).
[64] J. Li, J. Zhang, Q.S. Lu, Y. Yue, Y. Huang, D.W. Zhang, H.H. Lin, S.Y. Chen, X.Q. Yu. *Eur. J. Med. Chem.*, **44**, 5090 (2009).
[65] J.P. Kehrer. *Toxicology*, **149**, 43 (2000).
[66] P. Jogi, M. Padmaja, K.V.T.S. Pavan Kumar, C. Gyanakumari. *J. Chem. Pharm. Res.*, **4**, 1389 (2012).
[67] C.H. Ng, H.Ki.A. Ong, C.W. Kong, K.W. Tan, R.N.R. Rahman, B.M. Yamin, S.W. Ng. *Polyhedron*, **25**, 3118 (2006).
[68] E. Sundaravadivel, M. Kandaswamy, B. Varghese. *Polyhedron*, **61**, 33 (2013).